RESEARCH-ARTICLE

PolarVisor: Clutter-free, Electronics-free Fiducial Markers for mmWave Radars Printed on Paper

JUNBO ZHANG, Carnegie Mellon University, Pittsburgh, PA, United States

YIWEN SONG, Carnegie Mellon University, Pittsburgh, PA, United States

SWARUN KUMAR, Carnegie Mellon University, Pittsburgh, PA, United States

Published: 21 November 2025

Citation in BibTeX format

ACM MOBICOM '25: 31st Annual International Conference on Mobile Computing and Networking
November 4 - 8, 2025
Hong Kong, China

Conference Sponsors:
SIGMOBILE

ACM MOBICOM '25: Proceedings of the 31st Annual International Conference on Mobile Computing and Networking (November 2025)
https://doi.org/10.1145/3680207.3723456
ISBN: 9798400711299

PolarVisor: Clutter-free, Electronics-free Fiducial Markers for mmWave Radars Printed on Paper

Junbo Zhang
junboz2@alumni.cmu.edu
Carnegie Mellon University
Pittsburgh, PA, United States

Yiwen Song
yiwens2@andrew.cmu.edu
Carnegie Mellon University
Pittsburgh, PA, United States

Swarun Kumar
swarun@cmu.edu
Carnegie Mellon University
Pittsburgh, PA, United States

ABSTRACT

In this paper, we design and fabricate cost-effective, electronics-free millimeter-wave (mmWave) fiducial markers that support clutter-free detection on radars. Fiducial markers are widely used in camera-based systems to provide spatial information in robotic navigation applications. QR-code-like fiducial markers can be readily printed on paper – low-cost, easy to produce, and electronics-free. Yet, an analogous mmWave solution is yet to appear, which stems from the unique challenge in the mmWave context: its vulnerability to clutter. Existing solutions either trade hardware simplicity for clutter resilience or stay simple but remain vulnerable to environmental multipath. This paper seeks to solve this dilemma.

We introduce PolarVisor, where we imprint mmWave fiducial markers with paper and foils. Its key insight is manipulating signal polarization to enable clutter-free detection on its markers. Meanwhile, it builds on recent advances in passive metasurfaces where metallic patterns are readily hot-stamped on paper with foils. PolarVisor adopts an innovative design where the radar wears a visor (also paper-based) to eliminate clutter, leaving the markers readily visible. We include an in-depth analysis of its design and fabrication and we show that: (1) PolarVisor can support clutter-free detection at up to 25 m. (2) PolarVisor reports a self-localization accuracy of 0.0297 m (mean) and 0.0232 m (median) across multiple real-world, multipath-rich indoor environments.

CCS CONCEPTS

• **Hardware → Sensor applications and deployments**; **Wireless devices**.

KEYWORDS

Millimeter-wave, metasurface, polarization, localization

ACM MOBICOM '25, November 4–8, 2025, Hong Kong, China

ACM ISBN 979-8-4007-1129-9/2025/11.
https://doi.org/10.1145/3680207.3723456

ACM Reference Format:
Junbo Zhang, Yiwen Song, and Swarun Kumar. 2025. PolarVisor: Clutter-free, Electronics-free Fiducial Markers for mmWave Radars Printed on Paper. In *The 31st Annual International Conference on Mobile Computing and Networking (ACM MOBICOM '25), November 4–8, 2025, Hong Kong, China.* ACM, New York, NY, USA, 16 pages. https://doi.org/10.1145/3680207.3723456

1 INTRODUCTION

In this paper, we investigate a cost-effective, electronics-free design of fiducial markers for millimeter-wave (mmWave) radars by leveraging signal polarization. MmWave radars are widely used sensing platforms in automotive, robotic, and augmented reality (AR) applications. They are particularly invaluable when traditional optics-based sensing (e.g. cameras and LIDARs) fail due to occlusions such as mist or smoke. In this paper, we are interested in enabling mmWave-equipped platforms, such as robots or vehicles, to be able to locate themselves (i.e., self-localize) relative to pre-deployed, low-cost tags (markers) in the environment at fine-grained accuracy. We draw inspiration from AprilTags [38], printed on paper akin to QR codes that are used as similar fiducial markers for cameras (e.g., on AR headsets) to self-localize relative to the environment. Our proposed mmWave fiducial markers draw several key attributes from the simplicity of AprilTags: (1) Ultra-low-cost; (2) Printable on paper; (3) Entirely electronics- and battery-free; (4) Operating at ranges of several meters; (5) Enabling centimeter-level localization accuracy. Yet, quite unlike AprilTags, our design must be resilient to obstructions such as smoke or fog and operate within extremely cluttered environments.

Indeed, there have been several recent efforts to build tags to support RF localization at mmWave frequencies. Yet, none can offer the unique blend of simplicity and accuracy that AprilTags offer in the vision context. Much of the rich work on RF backscatter tags [6, 11, 31, 32, 34, 35, 37, 42, 50] would require a battery, increasing hardware complexity. More recent passive frequency-coded retroreflectors [1, 3, 7, 17, 20, 22–24, 27, 43–45] can be limited in range (e.g., a meter) and susceptible to multipath from ambient clutter, or require dedicated instruments like vector network analyzers (VNA). Therefore, we ask: can we build mmWave tags (markers) for

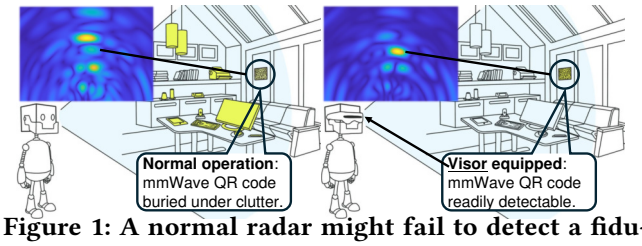

Figure 1: A normal radar might fail to detect a fiducial marker (an analogous mmWave QR code) due to background clutter. PolarVisor eliminates background reflectors with its visor, detecting only its markers.

self-localization that are cost-effective, completely passive, able to offer a range of several meters, and can operate in environments with high clutter?

We present PolarVisor, a passive design for mmWave fiducial markers that can be located from distances of several meters at centimeter-level accuracy, enabling robust radar self-localization in environments with high clutter. PolarVisor offers a passive and cost-effective design – made with paper and foils, it does not involve any electronics and supports rapid prototyping. Our detailed experiments show that PolarVisor can provide reliable clutter suppression and support clutter-free detection at up to 25 m; meanwhile, across multiple indoor test spaces, it reports a self-localization accuracy of 0.0297 m (mean) and 0.0232 m (median).

PolarVisor tackles a key challenge in designing entirely electronics-free tags for mmWave: ambient clutter. Specifically, in the absence of a battery, it is challenging to separate markers in the environment from other objects that also reflect radar signals. Telling markers apart from these background reflectors is not a problem unique to radars. In the realm of visual sensing, AprilTags are distinguishable from ambient objects owing to their special bar-code-like spatial structure (i.e., spatial coding). However, instrumenting passive RF tags with similar structures does not fundamentally solve the issue because there is no way to tell a "pixel" in the spatial code apart from background reflectors. Indeed, this is why traditional long-range mmWave tags are battery-powered in order to emit on/off codes and stand out from ambient clutter (i.e., temporal coding).

PolarVisor's secret sauce is to manipulate mmWave signal polarization. Generally, mmWave radars are equipped with microstrip patch antennas. They transmit and receive electromagnetic (EM) waves along one linearly polarized direction. Such design works well in practice because most target objects do not change signal polarization [16, 34]. While some structures with varied orientations (e.g., tree leaves) can scatter and depolarize radar signals, it happens in a random manner while also weakening the reflected signal significantly. Hence, they still manifest in the radar image, albeit as much fainter objects, and are usually not of interest. This opens up an opportunity: If we engineer the fiducial marker to deliberately shift the incident polarization by precisely 90° and observe along the perpendicular direction (i.e., cross-polar reception), we should only see the marker, while having nearly all other objects in the scene extremely faint, if not entirely invisible, in the radar image. Therefore, PolarVisor's main idea is to design a marker that deliberately shifts polarization, and then equip commodity radars with the ability to perform cross-polar reception that distinctly observes these markers with minimal hardware modification.

Specifically, PolarVisor consists of two main components: a marker that manipulates signal polarization and a visor that selects a certain polarization attached to the radar. It is loosely inspired by the "technical visors" envisioned in fiction and games – upon activating a visor at the radar, the background clutter is suppressed while the marker is sharply visible. As shown in Fig. 1, to a traditional radar, the PolarVisor marker and background reflectors appear together on the radar and may be hard to distinguish. However, with the visor "on", background reflectors are significantly suppressed, leaving the marker readily visible and locatable.

The rest of this paper discusses the key challenges in PolarVisor. First, designing a polarization-shifting reflector that can be printed on paper is not trivial. Without the manufacturing precision in printed circuit boards (PCB), polarization-shifting structures based on Van-Atta arrays [4, 6, 11, 21, 34, 35, 37, 50, 53] are hard to realize. PolarVisor draws from metasurfaces, where sub-wavelength structures are arranged on a surface to manipulate the amplitude and phase of EM waves. Specifically, a fast prototyping method has been proposed [15, 25, 33, 48] where paper, foils, and laminating machines are used to produce THz and mmWave metasurfaces with relatively simple structures. These single-layer metasurfaces are low-cost and electronics-free, but none of them can realize the function PolarVisor needs – completely shifting signal polarization by 90°. Meanwhile, researchers have looked into polarization-shifting structures (i.e., polarizers) [5, 8, 9, 14, 18, 28–30, 36, 40, 54, 56, 57, 62, 64], but their sophisticated, multi-layer designs are only realized with precise PCB prototypes. Can we build mmWave polarizers with high performance while being inexpensively printable on paper? In Sec. 4, we dive deep into the design of our marker (reflective polarizer) and visor (transmissive polarizer).

While a polarizer-based marker effectively suppresses clutter, it introduces a new problem: RF waves that bounce off its flat surface follow the laws of specular reflection. As a result, the cross-polar reflection from the PolarVisor marker will never be observed unless it perfectly faces the radar, rendering our design impractical. To resolve this, our marker must be re-designed to be retroreflective, i.e., it must reflect the radar signal along the incident direction. We build on the well-known retroreflective geometry of corner reflectors to achieve this. Specifically, we propose a corner reflector

with one face in the form of a reflective polarizer. In Sec. 5, we elaborate on this marker design.

Finally, we demonstrate how multiple PolarVisor markers work with the visor in synergy to facilitate self-localization in real-world environments in Sec. 6. Thanks to the clutter-free design, a PolarVisor marker is significantly easier to identify among background reflectors, making standard spatial coding (akin to bar codes) viable. PolarVisor hence performs spatial coding by arranging multiple markers that can be deployed at fixed and known locations within indoor spaces (e.g., attached to natural wall corners) to encode room/floor/building information. The radar, equipped with the visor, then moves around this indoor space and localizes itself by looking for pre-deployed spatial patterns of markers.

We detail PolarVisor's fabrication and experimental setup in Sec. 7 and we evaluate its performance with a COTS 24 GHz radar [10] in multiple real-world, multipath-rich environments in Sec. 8. PolarVisor achieves 0.0297 m (mean) and 0.0232 m (median) self-localization accuracy across three practical indoor test spaces. We include a comprehensive study of PolarVisor's performance where we vary multiple factors, such as range, blockage, and test environment. Meanwhile, we also investigate PolarVisor's clutter suppression performance with two micro-benchmarks. We show that a PolarVisor marker can suppress clutter and be robustly detected at up to 25 m from the radar. These promising results validate PolarVisor's unique and novel design.

2 PRIMER

In PolarVisor, metasurfaces manipulate mmWave signal polarization. We briefly introduce signal polarization (Sec. 2.1), metasurfaces (Sec. 2.2), and their connection (Sec. 2.3).

2.1 Polarization of Wireless Signals

RF signals are polarized in different ways. We limit our discussion to transverse EM (TEM) waves propagating in homogeneous, isotropic media as seen in mmWave radar contexts.

A propagating EM wave is essentially an EM field traveling along a certain direction $\hat{k}$. It can be further decomposed into an electric field $\vec{E}$ and a magnetic field $\vec{H}$ oscillating along the direction indicated by $\vec{E}$ and $\vec{H}$, respectively. According to Maxwell's equations, $\hat{k} \parallel \vec{E} \times \vec{H}$ follows right-handed law. The plane spanned by $\vec{E}$ and $\vec{H}$ is hence traverse to $\hat{k}$. We refer to this plane as the ***traverse plane***. Further, the direction of $\vec{E}$ is defined as the ***polarization direction***.

In practice, antennas determine the signal polarization. Common antennas (e.g., monopole, dipole, patch) all generate linear polarization, where $\vec{E}$ direction is time-invariant. If two such antennas orient perpendicularly to each other, they cannot talk to each other. This is referred to as ***polarization mismatch***. COTS mmWave radars generally adopt patch

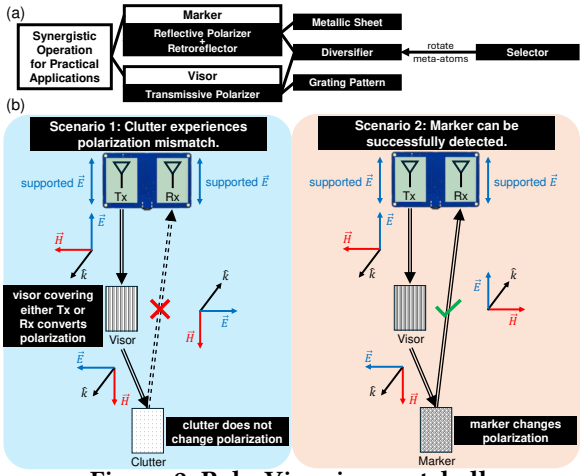

Figure 2: PolarVisor in a nutshell.

antennas, so their Tx and Rx antennas align to the same polarization direction. In other words, they support ***co-polar*** operations but not ***cross-polar*** operations.

2.2 Electromagnetic Metasurface

An electromagnetic metasurface refers to a surface (usually 2D) with specific repetitive elements that manipulates the properties of an incident EM wave, such as its amplitude, phase, and propagation direction. A simple intuition of its working principle is a macro-scale realization of individual micro-scale operating elements. The individual element, usually at a sub-wavelength scale, is also known as the ***meta-atom*** and interacts with an incident EM wave.

2.3 Metasurface Manipulating Polarization

How can a metasurface manipulate signal polarization? Here, we provide an intuitive example. Suppose we have an incident wave with $\hat{k} = -\hat{z}$ and a 45° linear polarization, i.e., its $\vec{E}$ can be decomposed into two equal-amplitude, in-phase components $\vec{E_x}$ along the x-axis and $\vec{E_y}$ along the y-axis (i.e., $\vec{E} = \vec{E_x} + \vec{E_y}$ and $\left\|\vec{E_x}\right\| = \left\|\vec{E_y}\right\|$). Now imagine a certain metasurface that does not react to $\vec{E_x}$ but selectively delays $\vec{E_y}$ by 180°, effectively flipping the sign of the field: $\vec{E_y}' = -\vec{E_y}$. The resulting electric field $\vec{E'} = \vec{E_x}' + \vec{E_y}' = \vec{E_x} - \vec{E_y}$ will be perpendicular to $\vec{E}$. This can also be interpreted as a counter-clockwise 90° shift on $\vec{E}$, so this metasurface is a polarization converter, or in short, a ***polarizer*** for $\vec{E}$ in effect.

This example shows how selectively manipulating the phase of electric field components effectively shifts polarization. In summary, designing a polarizer mainly explores: (1) how to realize selectivity along different directions; (2) how to apply the correct phase shift to the desired direction.

3 POLARVISOR OVERVIEW

PolarVisor is a cost-effective, passive fiducial marker solution for mmWave radars. As shown in Fig. 2(a), it has two important components: the marker and the visor.

Marker: A PolarVisor marker is a reflector that can distinguish itself from background reflectors by manipulating signal polarization. Therefore, it is both a reflector and a polarizer (i.e., ***reflective polarizer***). We further design it as a ***retroreflector*** to make it visible within a sufficiently large field of view across both azimuth and elevation angles.

Visor: A PolarVisor visor is designed to enable cross-polar reception on COTS radars, which by design only support co-polar reception. It is a planar structure with two sides (e.g., denote them as A and B). A and B are polarization filters allowing only certain polarization $\vec{E_A}$ or $\vec{E_B}$ to pass. An incident wave at A with $\vec{E_A}$ polarization is converted to its cross-polar direction $\vec{E_B}$ (i.e., $\vec{E_A} \perp \vec{E_B}$) before exiting from B. This process is reversible, so only EM waves with $\vec{E_B}$ polarization can enter from B and will be converted to $\vec{E_A}$ polarization before exiting from A. We call this a ***transmissive polarizer***, where a polarization conversion is cast on the EM wave passing through the structure. The visor is installed at either the radar transmitter (Tx) or receiver (Rx) – it should **not** cover both. In Fig. 2's example, it covers Tx, but covering Rx also works. The side (A/B) closer to the radar should share the same polarization as the antennas.

Relationship Between the Marker and Visor: Fig. 2(b) explains how PolarVisor works. When the radar is equipped with a visor (e.g., at its Tx), signals from the Tx are converted to the cross-polar direction immediately after transmission. Hence, signals in the environment are all cross-polar relative to the radar. Thus, background reflectors, which do not significantly change polarization, respond with cross-polar reflections. This will not be perceived by the Rx due to polarization mismatch. In contrast, the PolarVisor marker, as a reflective polarizer, converts polarization again in its reflection. This effectively shifts signal polarization back to the co-polar direction and hence will be perceived by the radar.

The PolarVisor marker and visor share the same building blocks – components we call ***diversifier*** and ***selector***. Hence, we organize our design sections following their architecture. In Sec. 4, we start by describing the selector (Sec. 4.1) and diversifier (Sec. 4.2), then build reflective polarizers (Sec. 4.3) and transmissive polarizers (Sec. 4.4) upon them. Next, in Sec. 5, we complete the PolarVisor marker as a retroreflector with a detailed geometric analysis.

End-to-end Operation: In Sec. 6, we describe how PolarVisor supports self-localization. Specifically, we leverage multiple markers to form a spatial code that embeds certain room/floor/building information similar to a QR code. Further, the mmWave radar, equipped with the PolarVisor visor, searches this known spatial pattern in an unknown environment. Upon detecting a certain pattern in its database, it localizes itself relative to the spatial code to infer its location.

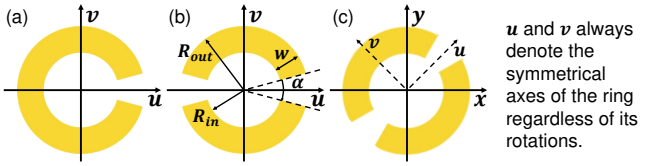

Figure 3: (a) A classical SRR. (b) A DSRR's parameters. (c) A DSRR rotated by 45° counterclockwise.

4 CRAFTING A PAPER POLARIZER

In this section, we walk through how a PolarVisor polarizer is built. While researchers have explored PCB polarizers, in PolarVisor, we design unique paper polarizers that offer high performance while being extremely tolerant of manufacturing imperfections. As mentioned in Sec. 2.3, a polarizer design breaks down into a metasurface that selects a certain polarization and a mechanism to apply a desired phase shift.

4.1 Selector: the Foundational Structure

PolarVisor's key building block is a selector – a meta-surface that permits only one polarization. Specifically, it is engineered to let signals polarized along one specific direction to pass through and the orthogonal direction to be reflected back. As we will later discuss, the selector is a foundational structure on which PolarVisor's other elements are built.

In PolarVisor, the selector is based on a variant of classical split ring resonators (SRR). Fig. 3(a) shows a classical SRR. It has two symmetry axes – the u-axis passing through the splits and the v-axis perpendicular to u. SRRs have been extensively studied in the metasurface literature. A metasurface with SRR meta-atoms is known to be capable of selecting polarization directions at its resonant frequencies – determined by its effective perimeter L_e and the wavelength λ [49].

Instead of a single split as seen in classical SRRs, PolarVisor implements two, which is sometimes called a double-split ring resonator (DSRR). However, we note that DSRR is also interchangeably used in the metasurface literature to refer to a pair of two single-split ring resonators, which is not the case for PolarVisor. The DSRR structure in PolarVisor possesses similar properties and its design procedure does not significantly differ from that of an SRR. In the following discussion, we denote its resonant frequency as f_c and it corresponds to the radar operating frequency.

For the DSRR in Fig. 3(b), upon perfect resonance at f_c, a u-polarized EM wave will be completely reflected, while a v-polarized EM wave can completely pass through. If we use r_{ij} to express the reflection coefficient where a j-polarized incident EM wave becomes an i-polarized reflection (i.e., j

to i conversion), then at f_c, $r_{uu} = 1$ and $r_{vv} = 0$. I.e., the metasurface acts as a mirror for u-polarized waves. We can also define the transmission coefficient t_{ij} where a j-polarized incident EM wave becomes an i-polarized wave after passing through the metasurface, then at f_c, $t_{uu} = 0$ and $t_{vv} = 1$, i.e., the metasurface is transparent for v-polarized waves.

While various meta-atom designs exist in the metasurface literature, PolarVisor's is designed for maximum tolerance of manufacturing imperfections.

(1) Meta-atom Shape: We recommend avoiding sharp corners – it is empirically observed in our fabrication that it is easier to produce round shapes than to imprint acute corners. Therefore, although L-shape resonators are also popular in the metasurface literature, we choose C-shape ones instead.

(2) Meta-atom Size: It is intuitive to understand that a smaller meta-atom generally leads to a smaller metasurface. Thus, to design a compact metasurface, if a meta-atom structure can meet a target effective perimeter while occupying less surface area, it should be preferred. In this case, structures based on SRRs are favored compared to simple rod or compass needle structures, although they have also been demonstrated as effective resonators in the literature.

(3) Trace Length: The SRR structure is a single metallic trace, which has a higher risk of breaking during manufacture. Hence, a DSRR structure is chosen.

(4) Printer Resolution: A printer's resolution translates to its DPI (dots per inch). To accommodate most printers, the trace in a meta-atom should not be too thin. This applies to the spacing between adjacent traces as well. In practice, we found an empirical value of 0.3 mm. It is recommended that both the trace width and spacing be larger than this value.

Table 1 shows PolarVisor's 24 GHz DSRR parameters.

Outer Radius R_{out}	2.4 mm	Ring Width w	1 mm
Inner Radius R_{in}	1.4 mm	Split Angle α	30°
Element Spacing P	7 mm	Metal Thickness h	40 µm

Table 1: Geometric parameters of PolarVisor's selector.

4.2 Diversifier: Building Block of Polarizers

What happens when the meta-atoms are rotated in a selector? The metasurface will become a ***diversifier*** – it generates diverse polarizations. This is the building block of polarizers.

Consider the 45° orienting meta-atom in Fig. 3(c). We define a new coordinate system x, y. In this paper, we keep u and v defined as the symmetry axes of the ring no matter how it rotates. Hence, in Fig. 3(c), $\hat{x} /\!/ \hat{u} - \hat{v}$ and $\hat{y} /\!/ \hat{u} + \hat{v}$.

An incident x-polarized wave $\vec{E}_x$ can be decomposed into two equal-amplitude components along u and v: $\vec{E}_x = \vec{E}_u + \vec{E}_v$ and $\left\|\vec{E}_u\right\| = \left\|\vec{E}_v\right\|$. Upon perfect resonance, $\vec{E}_u$ is completely reflected and $\vec{E}_v$ completely passes through. Hence, in effect, half of the incident power is reflected and the other half is transmitted. Further, since the reflection is $\vec{E}_u$, which can be re-written as $\vec{E}_u = \frac{\vec{E}_x}{\sqrt{2}} + \frac{\vec{E}_y}{\sqrt{2}}$, we know that half of the reflection is a u wave and the other half is a v wave. A similar analysis can be performed for the transmission. In summary, the 45° orienting meta-atoms form a "splitter": It splits the incident x wave into four quarters – a pair of co-polar reflection/transmission and a pair of cross-polar reflection/transmission. This provides a way to generate y components with pure x incidence and vice versa.

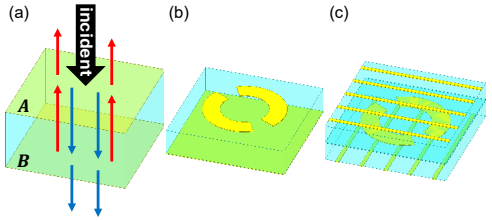

Figure 4: (a) A Fabry–Pérot cavity with two mirrors A and B at the top and bottom. (b) PolarVisor's reflective polarizer. (c) PolarVisor's transmissive polarizer.

4.3 Reflective Polarizer for Markers

A reflective polarizer is designed to reflect only and meanwhile change the polarization in the reflected wave. Yet, simply employing a 45° diversifier from Sec. 4.2 does not suffice, since it produces four E-field components. Instead, for an x incidence, we desire only the y reflection and wish to eliminate the other three. How can we achieve this?

PolarVisor leverages a concept widely used in optics and THz: the Fabry–Pérot resonant cavity [47]. Fig. 4(a) shows its basics. A Fabry–Pérot cavity consists of two reflective mirrors A and B facing each other and separated by a distance L_{FP}. EM waves enter the cavity (e.g., from A) and bounce back and forth. A and B are partially transmissive, allowing a small portion of waves to pass through. As the wave undergoes multiple reflections, constructive or destructive interference can happen inside the cavity. When a constructive one happens, the wave builds up and leads to a strong transmission at the exit B. When a destructive one happens, a strong reflection is observed at the entrance A. As one can imagine, the dominating interference depends on L_{FP}.

Now, imagine A being a 45° diversifier and B being a fully reflective metallic sheet. We can build a Fabry–Pérot-like cavity for polarization conversion purposes. Specifically, suppose we have an x incidence, and L_{FP} is chosen such that x components inside the cavity will keep bouncing until they are converted by the diversifier mirror to y components when they can finally exit the cavity, then such a cavity can effectively serve as an x-to-y polarizer. In this case, the cavity needs to make sure that the co-polar components not only vanish eventually inside but also experience a destructive

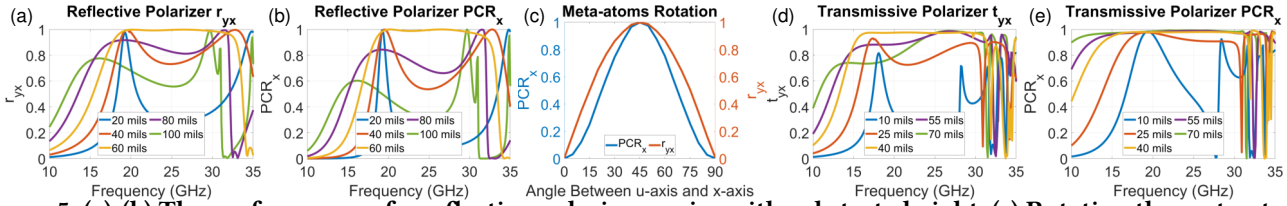

Figure 5: (a)-(b) The performance of a reflective polarizer varies with substrate height. (c) Rotating the meta-atoms changes polarizers' performance. (d)-(e) The performance of a transmissive polarizer varies with substrate height.

interference outside of A, such that the total field outside of the cavity is dominated by the cross-polar components.

Cavity Design: To see if an L_{FP} for such a cavity exists, we perform a simulation using ANSYS HFSS. We examine the x-to-y reflective coefficient r_{yx} and polarization conversion ratio (PCR) for x-to-y conversion $PCR_x = \frac{r_{yx}^2}{r_{yx}^2+r_{xx}^2}$. We vary L_{FP} (here, the substrate height) from 20 mils ($\approx 508\,\mu$m) to 100 mils ($\approx 2540\,\mu$m) with a step size of 20 mils.

As shown in Fig. 5(a) and (b), when L_{FP} is close to its optimal value (in this case, roughly around 60 mils $\approx 1524\,\mu$m), both r_{yx} and PCR_x are maximized. If L_{FP} is far from its optimal value, the performance becomes unstable, especially towards higher frequencies. In addition, the polarizer has a wide operating bandwidth when operating optimally. This is especially important since we are targeting a maximum tolerance of manufacturing imperfections.

For this reflective polarizer design, the required substrate height can be approximated by stacking multiple pieces of paper together. At first glance, one may wonder if such a method is inaccurate since an air gap might exist between adjacent pieces of paper. Hence, we carried out a simulation where a 100 µm-thick air gap insulates multiple layers of paper. The simulation results showed negligible diversion from Fig. 5(a) and (b). In practice, as we detail our fabrication in Sec. 7, air gaps are minimized by lamination sealing.

Optimizing the Diversifier: To better understand if our reflective polarizer design is optimal, we next analyze key design parameters for our diversifier. For example, we began with a diversifier with meta-atoms oriented at 45° – but is this choice optimal? Suppose in Fig. 3(c), the angle between unit vectors $\hat{u}$ and $\hat{x}$ is 30° instead of 45°. We will have $\hat{x} = \frac{\sqrt{3}}{2}\hat{u} + \frac{1}{2}\hat{v}$. Then, an x-polarized incident wave $\vec{E_i} = a\hat{x}$ with an amplitude of a can be re-written as $\vec{E_i} = \frac{\sqrt{3}}{2}a\hat{u} + \frac{1}{2}a\hat{v}$. The reflection will thus be $\vec{E_r} = \frac{\sqrt{3}}{2}a\hat{u} - \frac{1}{2}a\hat{v}$, which can be written in xy-coordinates as $\vec{E_r} = \frac{1}{2}a\hat{x} + \frac{\sqrt{3}}{2}a\hat{y}$. One can readily infer that instead of 90°, such a vector $\vec{E_r}$ is a 60° counterclockwise rotation of $\vec{E_i}$ with $PCR_x = (\frac{\sqrt{3}}{2})^2 = 75\%$.

We carry out a simulation where the angle between unit vectors $\hat{u}$ and $\hat{x}$ varies from 0° to 90°. As shown in Fig. 5(c), when this angle is 30°, the simulation indeed suggests a PCR of 75%, validating our analysis. Hence, reflective polarizer will only work as a 90° shifter if the incident EM wave has an equal-amplitude decomposition onto the u and v axes, meaning that a 45° diversifier is indeed the best choice.

4.4 Transmissive Polarizer for Visors

Designing a transmissive polarizer leverages Fabry–Pérot cavities as well – this time, we would like to maximize transmission at B instead of reflection at A in Fig. 4(a). To achieve this, PolarVisor leverages two cascaded Fabry–Pérot-like cavities to form a sandwich structure where a diversifier is in between two grate mirrors as shown in Fig. 4(c).

A grating pattern can be viewed as the simplest polarization selector. An incident wave with perpendicular polarization to the grate passes through. It is reflected otherwise. For an x incidence, an x-to-y polarizer has A as an x filter and B as a y filter. In this case, unconverted x components cannot exit at B. Meanwhile, successfully converted y components cannot escape from A but exit through B. The key to successful polarization conversion is controlling L_{FP} such that x components inside the cavity keep bouncing until they get converted to y components and exit the cavity at B.

Similar to Sec. 4.1, PolarVisor took multiple practical factors into consideration when designing its grating patterns.

(1) Pattern Choice: Since we need two semi-transmissive mirrors for surfaces A and B, at first glance, one may propose using the DSRR selectors in Sec. 4.1. In fact, we implemented this idea both in ANSYS HFSS simulations and in real-world fabrications and we observed complex coupling effects among these three layers of DSRR structures. As a result, the transmissive polarizer could not function as expected. One possible explanation for such a phenomenon could be that the resonant nature of DSRR structures would divert them from acting as pure semi-transmissive mirrors. Hence, we chose simple grates as semi-transmissive mirrors.

(2) Printer Resolution: The printer's DPI affects both the minimum possible trace width and spacing. We conducted an in-depth simulation where we studied the performance of the grating pattern relative to the width of individual grates w_g and the number of grates N in a single unit cell, which contains a single meta-atom and has a width/length of P. The grate spacing is then implicitly determined as P/N. The evaluation metric is intuitive: a better pattern corresponds to more transmission and less reflection. Our simulation

suggests: (a) w_g should be as thin as possible. (b) N should not be too large. While the latter is easy to satisfy and we set $N = 5$, PolarVisor sets w_g to be 0.3 mm, the thinnest possible trace that a general printer can handle – a practical constraint that does lead to some performance loss.

We verify our design in ANSYS HFSS. This time, the evaluation metrics are the x-to-y transmissive coefficient t_{yx} and the polarization conversion ratio $PCR_x = \frac{t_{yx}^2}{t_{yx}^2+t_{xx}^2}$. We let the two cascaded cavities have an equal L_{FP} (i.e., substrate height) and vary its value from 10 mils ($\approx$ 254 µm) to 70 mils ($\approx$ 1778 µm) with a step size of 15 mils ($\approx$ 381 µm). As shown in Fig. 5(d) and (e), when L_{FP} is close to its optimal value (around 40 mils $\approx$ 1524 µm), both t_{yx} and PCR_x are maximized. Again, an unstable performance is observed towards higher frequencies if L_{FP} is far from its optimal value. A similarly high bandwidth is seen at the optimal L_{FP}. This validates PolarVisor's polarizer design.

5 DESIGNING A RETROREFLECTOR

While the reflective polarizers in Sec. 4 hold promise in removing background clutter, a new issue arises. As a 2D planar structure, metasurfaces generally follow the law of specular reflection, similar to a mirror reflecting light. Since PolarVisor is not designed to induce phase shift gradient, it obeys this law. As a result, a reflective polarizer has a limited field of view – it is only visible when the mmWave radar is nearly perfectly facing it. It disappears with even a tiny misalignment, limiting the practicality of our design.

PolarVisor's solution is to implement ***retroreflective*** markers, which reflect EM waves along their incident direction. Since mmWave systems are designed to be highly directional, researchers have proposed various retroreflective structures, such as corner reflectors (CR), Van-Atta arrays, and Luneburg lenses. So which one works best for PolarVisor?

5.1 Determining a Retroreflective Structure

A Van-Atta array is an interconnected array of antennas where transmission lines are designed to inverse the phase gradient of an incident wave – a tiny fabrication mismatch could cause the reflection to faint. Hence, it is challenging for paper-based PolarVisor, which is expected to suffer from large manufacturing imperfections. Likewise, Luneburg lens, which relies on designing precise refractive index gradients, is hard to realize in PolarVisor as well.

Aiming at fast prototyping, PolarVisor thus adopts corner reflectors (CR). We construct CRs with a simple 3D-printed corner model (more in Sec. 7) for fast substitution of polarizer samples and easy installation. However, in practice, one can easily construct a CR with cupboard boxes or even by simply gluing sheets of paper together. This can greatly reduce the effort needed to construct a PolarVisor marker from scratch.

While normal CRs are well-known retroreflectors, will they work as polarization-converting retroreflectors if we attach a polarizer? Below, we detail our theoretical analysis.

5.2 Geometrical Analysis

We consider trihedral corner reflectors formed by three mutually perpendicular, intersecting flat surfaces. This geometry ensures that incoming radar waves are reflected multiple times within the structure, causing the waves to exit the reflector parallel to the direction they entered, regardless of the incident angle. CRs have been serving as reference targets in radar systems for calibrating the radar's accuracy and sensitivity because their radar cross section (RCS), although closely correlated with the physical dimensions, can be significantly larger [46]. The maximum RCS is reached when the radar illuminates the CR from the direction of the symmetry axis (i.e., boresight).

PolarVisor builds on top of a standard CR. Hence, it shares the pros and cons of common CR structures: (1) The RCS is fundamentally correlated to the physical size of the CR. (2) The radar has to illuminate the CR within its field of view, and vice versa, the CR has to be within the radar's field of view (both azimuth and elevation). In the following analysis, we assume the field of view condition.

Mathematical and physical analyses have shown that a normal CR does not change signal polarization during the multi-reflection process [16] – the electric field $\vec{E}$ may flip sign upon reflecting off a surface, but will not change its direction. Hence, to construct a polarizer CR, PolarVisor can substitute either one or three surfaces in a CR with a reflective polarizer to have an odd number of polarization conversions. However, note that our reflective polarizer is not an ideal, perfectly reflective surface – dielectric loss is inevitable when EM waves travel back and forth inside the substrate (paper). Hence, PolarVisor chooses to substitute only one of the three surfaces in a CR.

How should the reflective polarizer be oriented relative to the radar? To see why its orientation can make a difference, we look at Fig. 6. All objects are shown in their isometric view, and we assume the incident EM wave travels in the -z direction (i.e., $\hat{k} = -\hat{z}$) and is y-polarized (i.e., $\vec{E} /\!/ \hat{y}$). The radar faces the xy-plane (i.e., the traverse plane), having its patch antenna arrays aligning parallel to the y-axis (Fig. 6(a)). Consider a reflective polarizer (①) lying in the xy-plane with its symmetry axes u and v following $\hat{u} /\!/ \hat{x} + \hat{y}$ and $\hat{v} /\!/ -\hat{x} + \hat{y}$. This orientation leads to 100% polarization conversion.

To construct a CR while keeping $\hat{z}$ as the boresight direction, the reflective polarizer (①) will be rotated around the x-axis as shown in Fig. 6(b). The rotation angle $\theta = \arcsin \frac{\sqrt{6}}{3}$. Due to this rotation, vectors $\hat{u}$ and $\hat{v}$ are also rotated; hence, they are no longer in the xy-plane. The CR can be constructed

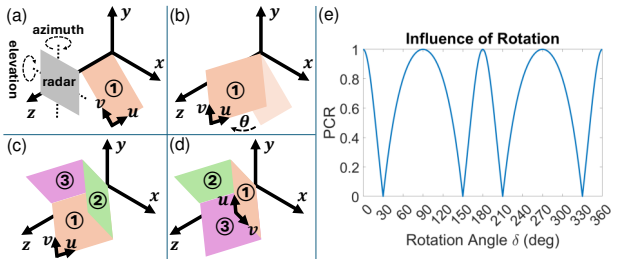

Figure 6: (a) A radar, whose traverse plane is parallel to the xy-plane, illuminates a reflective polarizer (①) with y-polarized signals. (b)-(c) To construct a polarization-converting CR, ① is rotated around the x-axis by θ, then we add two normal reflective surfaces (② and ③). The CR's boresight direction aligns with the z-axis. (d) The CR is further rotated around the z-axis by 120°. (e) Simulation result of traverse plane rotation.

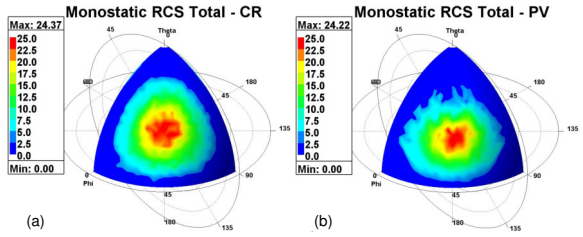

Figure 7: The RCS of (a) a normal CR and (b) a PolarVisor marker (polarization-converting CR).

by adding two normal reflective surfaces (② and ③) as in Fig. 6(c). In this case, if an EM wave is incident along -z, the CR should be able to achieve its maximum RCS. To verify that it still functions as a corner reflector, we carried out a simulation study in ANSYS HFSS. As shown in Fig. 7, with the same dimensions, the total RCS of our polarization-converting CR structure is roughly the same as a normal CR. This indicates that replacing one surface of a CR structure with a reflective polarizer does not impact its function as a corner reflector.

What happens to the polarization? As one can imagine, since its propagation direction $\hat{k}$ is not perpendicular to the polarizer surface, analyzing its polarization boils down to projecting its electric field onto the polarizer plane. More specifically, we need to calculate the inner products $\langle \vec{E}, \hat{u} \rangle$ and $\langle \vec{E}, \hat{v} \rangle$ to determine the respective strengths along the symmetry axes of the polarizer. If these two components have an equal amplitude (i.e., $\left\| \langle \vec{E}, \hat{u} \rangle \right\| = \left\| \langle \vec{E}, \hat{v} \rangle \right\|$), then the reflective polarizer can operate as expected. For Fig. 6(c), this holds true. It can be intuitively understood by looking at the yz-plane and the metasurface plane. Since they are perpendicular to each other and $\vec{E}$ is a vector in the yz-plane, its projection onto the metasurface plane will align with $\hat{u} + \hat{v}$. Hence, the reflective polarizer works as usual. Next, we analyze the impact of four possible radar movements.

Linear Translation: If the radar moves along the x, y, or z axis, it will no longer illuminate the CR from its boresight direction (i.e., $\hat{k} \neq -\hat{z}$), leading to a decrease in the observed RCS. Yet, as long as the radar is readily in the field of view of the CR (and vice versa), the CR will still function as a retroreflector and will be observed. Meanwhile, since the electric field still aligns with the y-axis (i.e., $\vec{E} \,/\!/\, \hat{y}$), the inner products $\langle \vec{E}, \hat{u} \rangle$ and $\langle \vec{E}, \hat{v} \rangle$ remain unchanged. Hence, the reflective polarizer will function as expected.

Azimuth Rotation: An azimuth rotation is equivalent to a rotation around the y-axis. Again, the radar will no longer illuminate the CR from its boresight direction. Yet, if we assume that the radar is in the field of view of the CR and vice versa, the CR will still function. In addition, since such a rotation around the y-axis does not change the direction of the EM wave, we still have $\vec{E} /\!/ \hat{y}$. Therefore, the inner products will still have an equal amplitude (i.e., $\left\| \langle \vec{E}, \hat{u} \rangle \right\| = \left\| \langle \vec{E}, \hat{v} \rangle \right\|$), and the reflective polarizer will function as expected.

Elevation Rotation: As seen in Fig. 6(a), the axis which an elevation rotation happens around is parallel to the x-axis. In this case, the radar plane will always be perpendicular to the yz-plane no matter how it rotates. Therefore, although the incident electric field $\vec{E}$ might no longer be parallel to the y-axis, the inner products $\langle \vec{E}, \hat{u} \rangle$ and $\langle \vec{E}, \hat{v} \rangle$ will still have an equal amplitude. The reflective polarizer thus will function.

Traverse Plane Rotation (Polarizer Installation): Finally, we consider rotating the radar within the traverse plane (i.e., around the z-axis). When there is only one object of interest (i.e., the CR), this is equivalent to rotating the CR around the z-axis. In addition, it also coincides with analyzing the CR where the same polarizer is not installed on the bottom surface (①) as in Fig. 6(b) but on one of the other two surfaces. As shown in Fig. 6(d), it is equivalent to rotating the CR in Fig. 6(c) around the z-axis by $\delta = 120°$ counterclockwise. In this case, $\hat{v}$ is parallel to the yz-plane. A simple calculation reveals that $\left\| \langle \vec{E}, \hat{u} \rangle \right\| = \frac{1}{2} \left\| \langle \vec{E}, \hat{v} \rangle \right\|$, leading to a PCR of 80%.

The above example shows that a CR with one of its surfaces as a reflective polarizer should not be rotated after installation. This can be intuitively explained as a result of breaking the symmetry of a CR – around the z-axis, it is no longer rotational symmetric. Will this be an issue?

We carry out a simulation study in MATLAB where we rotate the CR in Fig. 6(c) around the z-axis by an angle of $\delta \in [0°, 360°]$. Fig. 6(e) shows the PCR experiences fluctuation, where a low PCR indicates reduced polarization conversion. In practice, it is very unlikely that a radar will rotate within the traverse plane drastically during normal operation, e.g., when it is mounted on a platform like a car or a robot. Thus, the variation in PCR does not have a significant impact from a deployment perspective. However, we acknowledge this

limitation in Sec. 9 and evaluate traverse plane rotation as a micro-benchmark in Sec. 8.8. We show that the range of δ in which our marker works as expected is reasonably large. When deploying a marker, one only needs to make sure it is installed with an appropriate choice of δ.

6 DEPLOYING POLARVISOR IN PRACTICE

In this section, we describe how PolarVisor markers work as equivalent pixels in an analogous mmWave QR code. The clutter-free design of each marker unlocks spatial coding for PolarVisor, which can be challenging for normal reflectors, especially in highly cluttered scenes. With its visor clearing out background reflectors, PolarVisor can readily identify a spatial pattern formed by multiple markers. We note that spatial coding has been explored in multiple fields (e.g., cameras [38] and mmWave [19]) and there have been dedicated papers to study its design and performance. In PolarVisor, we complete the system with a simple form of spatial coding, but the design of spatial codes is not considered as a main contribution and hence is not evaluated separately.

6.1 Spatial Code Functions

In PolarVisor, we form an analogous mmWave QR code by arranging mmWave reflectors according to a specific 2D/3D pattern to provide the following two functions.

Identification: Contextual information, such as geometric information (e.g., room/floor) or navigation information (e.g., stop/detour), can be embedded. For example, an L shape can be formed with 3 reflectors to represent "lobby", or a cross with 5 reflectors can indicate "no trespassing". As this is not related to PolarVisor's performance, it is not evaluated.

Localization: Spatial codes are deployed at known locations. In addition, in a certain spatial code, the relative positions between markers are also known. This information (e.g., coordinates of each marker), along with other necessary complements (e.g., maps and floor plans), is stored in a database. Later, when a radar tries to perform self-localization, upon successful detection of a certain spatial code, it first estimates its relative position w.r.t. this code, then queries the database to fetch the location of this code, and finally combines these two to figure out its location.

6.2 Practical Operation

During a practical operation, the radar roams around a scene and tries to localize itself by detecting spatial codes that are pre-deployed. This is a two-step procedure. It starts by detecting potential markers, then tries to reconstruct spatial codes in its database with these detected markers.

Recording Potential Markers: As one can imagine, there is no mechanism for the radar to tell between a PolarVisor marker and a normal reflector if the latter is strong enough to stand out even after suppression (which will then significantly contribute to the localization error). Hence, the radar would simply look at all strong targets and record their relative positions w.r.t. itself. Further, it updates the recorded relative positions by tracking its own movement with the help of other sensing units (e.g., IMU modules).

Reconstructing Spatial Codes: The radar tries to reconstruct spatial codes in the database with some or all of the recorded markers. For example, if the radar has detected four potential markers and there is an L-shape code with three markers is in its database, it will try to form a similar L-shape code using three of the four potential markers. This might not succeed because the L-shape code in the database requires the markers to arrange according to predetermined relative positions (as mentioned in Sec. 6.1) – in that case, the radar will simply proceed and try to detect more potential markers. Note that this procedure does not necessarily require that all markers that make up a certain spatial code manifest simultaneously. For example, if a rectangular code has its markers deployed at the four corners of a wall, the radar might not see all of them at once. However, since the radar tracks its relative position to all detected potential markers, it can try reconstructing a spatial code at any time.

Evaluating PolarVisor: We consider several real-world, multipath-rich environments. In each environment, we deploy a spatial code with a certain number of reflectors at known locations. The location of this spatial code can be defined as the center of all reflectors. Meanwhile, we evaluate two systems – a baseline system, where the reflectors are normal CRs, and PolarVisor, where the reflectors are PolarVisor markers. In either of the two, the radar first tries to detect potential markers, then tries to reconstruct the spatial code with detected markers. Once it determines that it has successfully reconstructed the spatial code, it outputs the estimated location of itself. The localization error is calculated as the difference between this esimated location and the true location obtained with laser rangefinders. Compared to the baseline, PolarVisor is expected to be less vulnerable to background clutter, and hence should have a higher chance to reconstruct the spatial code with PolarVisor markers (instead of mistakenly using background reflectors).

7 IMPLEMENTATION

7.1 Fabrication

Metasurfaces: Multiple fabrication methods exist for metasurfaces, including PCB drilling [39], laser cutting [52], 3D-printed PCB [55], microfluidic circuit [13], CVD [61], and LPD [66]. We chose hot-stamping due to its low cost and the flexibility of paper substrates. We envision that similar to fiducial markers for cameras, PolarVisor can also be made and used easily. To start, single-layer metasurface patterns

are first printed with a laser printer (Konica Minolta Bizhub 300i) on 48-pound glossy brochure paper (HP Q1987A). Next, we place a heat transfer foil (Cricut) on top of the printer pattern and stack another piece of 48-pound paper. This sandwich structure is fed into a laminating machine (SINCHI ProLami F3410) using the 10-mil lamination mode. After the foil cools down, we gently peel it off to get a paper metasurface.

Reflective Polarizer: A reflective polarizer has three basic layers from top to bottom. (1) A diversifier metasurface: A single piece of printer paper, facing up. (2) Substrate: We find the best configuration is stacking 5 pieces of 65-pound paper (Recollections Cardstock Paper). (3) A metallic sheet: We use the same heat transfer foil as this reflective layer, with its shiny face facing down. All materials are trimmed to a proper size before we put them into a 3-mil laminating pouch and perform a standard lamination. Each reflective polarizer in PolarVisor measures 5.5×5.5 inch^2.

Transmissive Polarizer: A transmissive polarizer has six layers. (1) A grating pattern: A single piece of printer paper, facing up. (2) Substrate: We recommend stacking 3 pieces of 65-pound paper, or alternatively, stacking 2 pieces of 110-pound paper. (3) A piece of blank glossy printer paper to ensure structural symmetry. (4) A diversifier metasurface: A single piece of printer paper, facing up. (5) Substrate: Another stack of thick paper, identical to step (2). (6) A grating pattern: Perpendicular to the one in step (1), facing down. We then trim, seal, and laminate same as above. Each transmissive polarizer in PolarVisor also measures 5.5×5.5 inch^2.

Corner Reflectors: We 3D-print a corner mold with three mutually perpendicular faces, each measuring 3 mm in height and 15 cm in width/length. A single piece of reflective polarizer is installed on one of the inner walls. On the other two, we install reflective surfaces – we trim a piece of heat transfer foil, encapsulate it in a laminating pouch, and perform a standard lamination. To better hold the CR, a 3D-printed base is attached by hot gluing to facilitate deployment.

7.2 Experimental Setup

Radar: We evaluate PolarVisor's performance with EVAL-TINYRAD from Analog Devices [10]. It operates within 24-24.25 GHz with 2 Tx and 4 Rx antennas co-located. We cover only its Tx with the visor (as shown in Fig. 2).

Environments: We consider 3 indoor environments (Fig. 8(b)-(d)). (1) A conference room: There is a slight blockage from the tables. The metallic window frames and the table legs contribute to clutter. (2) An office: It has relatively scattered background reflectors. (3) A lab space: It is densely occupied with tables, shelves, and equipment. In addition, a fourth testbed, a semi-indoor parking complex on the university campus (photo omitted), is used for blockage experiments and micro-benchmarks since our blockage experiments involve a fog generator, which cannot be used indoors.

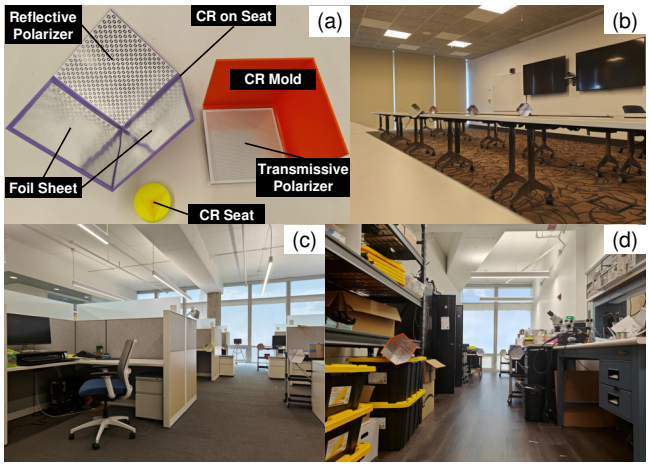

Figure 8: (a) PolarVisor components. (b)-(d) Test environments with clutter – a conference room, an office, and a lab. Four markers are shown in each photo.

8 EVALUATION

8.1 Localization: Evaluation Metric

In Sec. 8.2, 8.3, 8.4, and 8.5, we evaluate PolarVisor's localization performance. As outlined in Sec. 6.2, we evaluate PolarVisor with PolarVisor markers and a baseline system with normal CRs. As the radar moves to different locations, both systems try to reconstruct predetermined spatial codes with detected reflectors and report their self-localization estimates. We calculate the localization error at each radar location using their self-localization estimate and their true position (obtained using laser rangefinders). Each environment is evaluated in a semi-static manner – the radar moves along a fixed trajectory with roughly 20 predetermined locations and captures 10 frames at each location. We then report the cumulative distribution function (CDF) of this error.

8.2 Localization in Different Environments

Method: We deploy spatial codes with 3 or 4 reflectors in the conference room, office, and lab environment.

Result: In Fig. 9(a), 3 reflectors are used. We see that the baseline has higher errors across all 3 environments. Meanwhile, PolarVisor is confused by a strong background reflector in the lab even after clutter suppression. It reports an average error of 0.0557 m, 0.0426 m, and 0.0639 m for the conference room, office, and lab environment, respectively, while the baseline reports 0.211 m, 0.392 m, and 0.238 m. The issue is resolved in Fig. 9(b) with 4 reflectors. The localization accuracy of both PolarVisor and the baseline is considerably improved, while PolarVisor still outperforms the baseline across all environments. Specifically, the average localization

errors are 0.0279 m, 0.0290 m, and 0.0322 m for PolarVisor and 0.0693 m, 0.064 m, and 0.07 m for the baseline.

8.3 Localization with Multiple Markers

Method: We deploy spatial codes consisting of up to 7 reflectors in the lab environment.
Result: As shown in Fig. 10(a), when the number of markers increases from 2 to 5, an impressive improvement in localization accuracy is observed. However, since in PolarVisor, we do not deliberately implement angular resolution enhancement techniques (e.g., synthetic apertures), reflectors in the environments cannot be placed too close to each other – otherwise, they cannot be independently detected. Hence, the radar will only see a subset of markers at a time even when abundant markers are deployed (Sec. 6.2). A complex spatial code with more markers can help the radar robustly detect and identify the code, but the improvement gradually becomes marginal. More advanced spatial codes can further improve PolarVisor's performance (Sec. 9).

8.4 Localization with Blockage

Method: Normal reflectors are known to be operable under blockage for mmWave radars, so in this experiment, we only consider PolarVisor. We consider four types of blockage: (1) Fog generated from a fog machine using fog liquids. (2) Clear acrylic sheet (5 mm thick). (3) Wood board (2 mm thick). (4) Cardboard delivery package box (3 mm thick). We deploy 3 markers in the parking complex due to security considerations (dense fog may trigger indoor fire alarms).
Result: As shown in Fig. 10(b), different blockages do not pose a significant challenge. The acrylic sheet is relatively thick (5 mm) and hence it slightly affects PolarVisor's performance. Overall, PolarVisor remains robust across different NLOS scenarios where it is expected to operate robustly.

8.5 Localization vs Varying Range

Method: We deploy spatial codes with 3 reflectors in the office and lab and sample the scene with different spatial code locations, leading to different distances to the radar.
Result: Fig. 11 shows the comparison between PolarVisor and the baseline where we group the range values into bins of 1 m. At first glance, one will intuitively think the distance from the reflectors to the radar will impact the localization accuracy because a farther reflector will have a weaker strength detected by the radar. This is verified in the baseline results – when the normal CRs are farther from the radar, the localization error is slightly worsened. Meanwhile, we see PolarVisor does not fluctuate much across different ranges. This can be attributed to its clutter-free design. Although the PolarVisor markers will also become weaker in strength as they get farther from the radar, as long as the background clutter is suppressed, it is not negatively impacted.

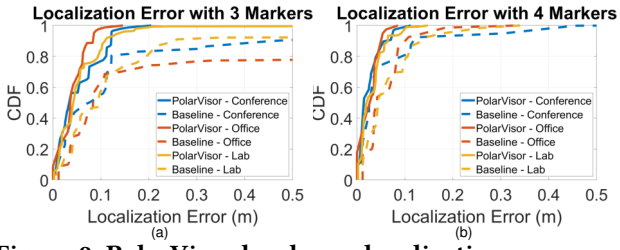

Figure 9: PolarVisor has lower localization error compared to the baseline across three real-world indoor environments with (a) 3 markers and (b) 4 markers.

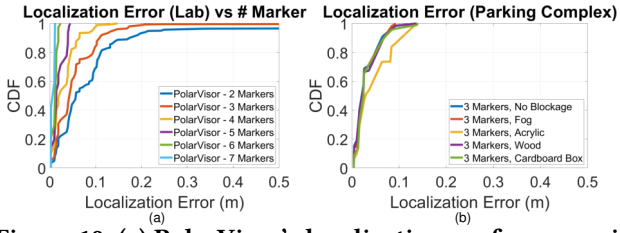

Figure 10: (a) PolarVisor's localization performance in the lab environment with up to 7 markers. (b) PolarVisor remains robust in multiple NLOS scenarios.

Large variances are observed in both PolarVisor and the baseline. This is because the distance between the reflectors and the radar is not the only factor impacting the localization accuracy – in fact, a more significant impact comes from the location of background reflectors. If some of them are very strong, then no matter where we place our spatial code, the radar will be misled. Since we do not deliberately control this, they can appear anywhere, making the variance large. Meanwhile, we see PolarVisor has a lower variance compared to the baseline, indicating a more stable performance.

8.6 Clutter Suppression: Evaluation Metric

In Sec. 8.7 and 8.8, we evaluate PolarVisor's clutter suppression performance with two micro-benchmarks. We analyze a single reflector in the parking complex, where we roughly align the radar along the reflector's boresight direction. We consider the following three scenarios. ⓐ: A normal CR and a normal radar. ⓑ: A normal CR and a visor-equipped radar. ⓒ: A PolarVisor marker and a visor-equipped radar.

We first define ***relative amplitude*** as the reflector's signal strength on the radar after background noise subtraction to see how strong the reflector manifests. Next, we define ***reflector suppression*** as the difference of relative amplitude between ⓐ and ⓑ to visualize how much a normal CR is suppressed because of the visor. Finally, we define ***clutter contrast*** as the difference of relative amplitude between ⓑ and ⓒ to show how much brighter a PolarVisor marker is

compared to a normal CR with visor equipped. State-of-the-art markers without cross-polarization do not separate themselves from clutters as reported in [50].

8.7 Suppression vs Varying Range

Method: In this micro-benchmark, we evaluate the influence of distance (i.e., range) between the radar and a single reflector – a normal CR or a PolarVisor marker. We report *reflector suppression* and *clutter contrast* w.r.t. distance.
Result: As shown in Fig. 12(a), PolarVisor can successfully suppress clutter at a range of up to 25 m. We did not evaluate beyond 25 m because the normal CR already performed similarly to obstacles near the radar (e.g., load-bearing pillars in the parking complex). The reflector suppression curve shows an average of 17.87 dB clutter suppression. Meanwhile, the clutter contrast curve indicates an average gain of 9.49 dB across all distances. The effective total gain curve is calculated as the sum of these two, whose intuition is a combination of the suppression we get from the visor and the gain we get from the marker. It drops slightly when the distance is far, but largely remains more than 20 dB.
Summary: An average of 17.87 dB clutter suppression validates our visor design – it is very effective in suppressing normal reflectors. Meanwhile, an average of 9.49 dB clutter contrast ensures that a PolarVisor marker is always significantly brighter than a suppressed normal reflector.

8.8 Suppression vs Traverse Plane Rotation

Method: In this micro-benchmark, we evaluate the influence of traverse plane rotation. Since there is only one reflector, rotation of the radar is equivalent to that of the reflector. We deploy the reflector at three different distances from the radar and perform a 360° traverse plane rotation with a rotary motor. We report the relative amplitude w.r.t. the rotation angle. We consider ⓑ and ⓒ – since the visor is on for both, any discrimination between them reveals the difference between a normal surface and a polarizer, and the main goal of this micro-benchmark is to see this difference.
Result: As shown in Fig. 12(b), a PolarVisor marker (PV, ⓒ) experiences more fluctuation compared to a normal CR (ⓑ). As the distance between the radar and the reflector increases, both objects appear weaker, but ⓒ is still brighter than ⓑ. Certain δ values, at which the marker appears weaker than a normal CR, can be due to the imperfection of our polarizers.
Summary: The observed pattern validates our analysis in Sec. 5 Fig. 6(e). We will have more discussion in Sec. 9.

9 DISCUSSION

Practical Visor Operation: Although cross-polarization can be easily achieved by re-designing the radar PCB, PolarVisor chose a visor design to avoid altering COTS radars.

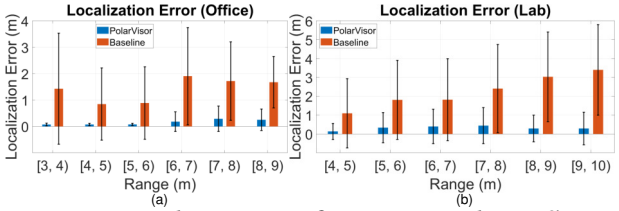

Figure 11: Localization performance with 3 reflectors in the (a) office and (b) lab environment where we vary the distance from the reflectors to the radar (range).

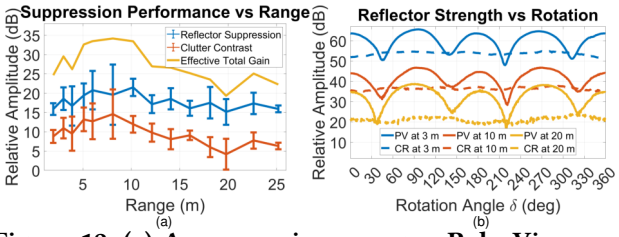

Figure 12: (a) Across various ranges, PolarVisor provides reliable clutter suppression. (b) PolarVisor experiences fluctuation with traverse plane rotations.

More importantly, the radars can still function normally when the visor is off. In practice, when a radar-equipped robot is in action, mechanical systems (e.g., robotic arms) can be implemented to help the radar wear the visor only when needed to support both co-polar and cross-polar operations.
Radar and CR Intrinsic Limitations: PolarVisor currently builds on COTS radars and standard CRs; hence, it shares their intrinsic limitations: (1) PolarVisor's scalability is limited by radar angular resolution. However, algorithms that improve angular resolution can help PolarVisor deploy dense markers to support high-density localization. (2) PolarVisor markers, as CRs, cannot support extremely slanted viewing angles. (3) Although PolarVisor remains robust with blockage (Sec. 8.4), extremely cluttered and dynamically obstructed environments are still challenging; we plan to further improve and evaluate PolarVisor there as future work.
Rotational Symmetry: As we have elaborated in Sec. 5, a PolarVisor marker does not have rotational symmetry along its boresight direction. Hence, its installation should follow Fig. 6(e) to ensure it operates correctly. Meanwhile, this also implies that the radar should not rotate drastically within the traverse plane. Although a radar with a fixed position (e.g., mounted on a car or a robot) is unlikely to experience such a rotation, we admit that a handheld device is an exception. In application scenarios where an operator holds the device, PolarVisor can seek help from inertial measurement units (IMU) and guide the operator to adjust the device's orientation for a live scan. Meanwhile, an alternative approach is to leverage spherical structures (e.g., lens) and wrap a PolarVisor polarizer around. New design and fabrication challenges will arise there and we leave it as future work.

Spatial Coding: Although PolarVisor, in its current form, does not include an in-depth investigation into spatial code design, we believe this can be an important future direction. A properly designed spatial code can potentially improve PolarVisor's localization performance. For example, if a certain arrangement of reflectors is unlikely to appear for background reflectors, then PolarVisor has a higher chance to correctly identify the markers constituting this spatial code.
System Complementation: PolarVisor can complement multiple mmWave methods. For example, radar adaptive beamforming [12, 51] can improve the signal quality from specific directions, from which PolarVisor can benefit if the marker is beamformed towards. Machine learning [26] and super resolution algorithms [41] can also improve the detection accuracy and working range of PolarVisor. Electronically-assisted and frequency-coded [58] design can improve PolarVisor's performance, if an ultra-long range is needed.

10 RELATED WORK

MmWave Backscatter: There has been extensive research on mmWave backscatter communication where low-power tags modulate their reflection with information bits (i.e., temporal coding) [6, 11, 31, 32, 34, 35, 37, 42, 50]. A chip and a battery are commonly seen because these tags are dedicated to communicating arbitrary information. Retroreflective structures are also widely used to compensate for the well-known high path loss in order to improve communication range, such as Van-Atta arrays [6, 11, 17, 34, 35, 37, 50] and Luneburg lenses [42]. PolarVisor focuses on a solution for fiducial markers where it only needs to convey predetermined geometric and spatial information instead of arbitrary bits. This opens up an opportunity to implement markers without chips and batteries, but only with paper and foils, highlighting a convenient, cheap, and unique manufacturing procedure rarely seen in the literature.
Passive mmWave Retroreflectors: Passive retroreflectors, even without embedded bit information, are shown capable of supporting a variety of sensing applications, such as corner reflectors (CR) [59, 60] and Van-Atta arrays [4, 21, 53]. To further encode information, frequency coding has been identified as an alternative to temporal coding when a battery is not present. This includes CRs [27, 44, 45], lenses [3, 7, 20, 22–24, 43], reflectarrays [17], and resonator arrays [1]. In addition, [19] implements spatial coding with CRs in a compact form factor. Since frequency coding is sensitive to environmental multipath, PolarVisor adopts spatial coding. On top of that, it leverages signal polarization to improve the detection of PolarVisor markers even in cluttered scenes. Compared to previous solutions, PolarVisor features achieving clutter resilence at a longer range (several meters) with COTS hardware instead of dedicated instruments like VNAs.
Metasurfaces: PolarVisor is closely related to passive metasurfaces (i.e., without active components), in which a rich literature exists. PolarVisor draws its inspiration on metasurface manufacture from [15, 25, 33, 48], which introduced and demonstrated an effective and convenient approach of prototyping single-layer metasurfaces with paper, foils, and laminating machines. Meanwhile, PolarVisor's meta-atom has a double split-ring resonator structure (DSRR), which is based on the classical split-ring resonator (SRR) that has been demonstrated to have a good performance for mmWave and THz applications [28, 49, 56, 63]. We build upon this literature and propose to use metasurface polarizers as the building block for clutter-free, electronics-free fiducial markers.
Polarization Manipulation: While signal polarization has been explored in mmWave communication as a potential way to perform MIMO, it has been studied for sensing applications as well, for example, [2, 17, 65] design mmWave polarization tags. Polarization manipulation is also a hot topic in metasurface research. Multiple passive polarizer designs have been proposed for microwave [8, 9, 18, 28–30, 36, 64], mmWave [5, 56], and THz [14, 40, 54, 57, 62] applications. PolarVisor builds upon these and dedicates its efforts to designing passive, clutter-free fiducial markers where it does not enjoy the precise manufacturing process commonly seen in printed circuit board (PCB) technologies.

11 CONCLUSION

In this paper, we present PolarVisor, an electronics-free fiducial marker solution for mmWave radars to support accurate, clutter-free robotic self-localization applications without any hardware modification to COTS mmWave radars. PolarVisor designs passive, polarization-manipulating metasurfaces that can be rapidly manufactured with paper and foils without any electronics or batteries. It adopts an innovative design where the radar wears a visor as a polarization filter to significantly suppress background reflectors while highlighting PolarVisor markers in the scene. An in-depth evaluation shows that PolarVisor can provide robust clutter suppression at a range of up to 25 m. Meanwhile, a comprehensive investigation into its localization accuracy reveals 0.0297 m (mean) and 0.0232 m (median) localization error across multiple real-world, multipath-rich indoor environments.

ACKNOWLEDGMENTS

We acknowledge the support of NSF (2106921, 2030154, 2007786, 1942902, 2111751), ONR, AFRETEC, MFI, CISCO, and CyLab-Enterprise. Any opinions, findings, and conclusions or recommendations expressed in this material are those of the author(s) and do not necessarily reflect the views of the above. We also thank the shepherd and reviewers for their help in improving this material.

REFERENCES

[1] Ali Alhaj Abbas, Aman Batra, and Thomas Kaiser. 2024. Chipless Tag Identification in Cluttered Environments through mm-Wave SAR Imaging. In *2024 15th German Microwave Conference (GeMiC)*. 185–188. https://doi.org/10.23919/GeMiC59120.2024.10485305

[2] Ali Alhaj Abbas, Mohamed Haj Hassan, Ashraf Abuelhaija, Daniel Erni, Klaus Solbach, and Thomas Kaiser. 2021. Retrodirective Dielectric Resonator Tag with Polarization Twist Signature for Clutter Suppression in Self-Localization System. *IEEE Transactions on Microwave Theory and Techniques* 69, 12 (dec 2021), 5291–5299. https://doi.org/10.1109/TMTT.2021.3108151

[3] Ali Alhaj Abbas, Yamen Zantah, Ashraf Abuelhaija, and Thomas Kaiser. 2022. Millimeter-Wave Retro-Directive Frequency Coded Lens by Curved One-Dimensional Photonic Crystal Resonator. *IEEE Access* 10 (2022), 132988–133000. https://doi.org/10.1109/ACCESS.2022.3226124

[4] Paris Ang and George V. Eleftheriades. 2018. A Passive Redirecting Van Atta-Type Reflector. *IEEE Antennas and Wireless Propagation Letters* 17, 4 (apr 2018), 689–692. https://doi.org/10.1109/LAWP.2018.2812108 arXiv:1803.02856

[5] Amjad Aziz, Babar Kamal, Zakriya Faraz, Usman Ali, Sadiq Ullah, Yingzeng Yin, and Jian Ren. 2024. Wideband and high efficient polarization conversion and RCS reduction based on compass needle shape metasurface. *Optics & Laser Technology* 177 (oct 2024), 111145. https://doi.org/10.1016/J.OPTLASTEC.2024.111145

[6] Kang Min Bae, Hankyeol Moon, Sung-Min Sohn, and Song Min Kim. 2023. Hawkeye: Hectometer-range Subcentimeter Localization for Large-scale mmWave Backscatter. In *Proceedings of the 21st Annual International Conference on Mobile Systems, Applications and Services* (Helsinki, Finland) *(MobiSys '23)*. Association for Computing Machinery, New York, NY, USA, 303–316. https://doi.org/10.1145/3581791.3596869

[7] Ryan A. Bahr, Ajibayo O. Adeyeye, Samantha Van Rijs, and Manos M. Tentzeris. 2020. 3D-Printed Omnidirectional Luneburg Lens Retroreflectors for Low-Cost mm-Wave Positioning. In *2020 IEEE International Conference on RFID (RFID)*. 1–7. https://doi.org/10.1109/RFID49298.2020.9244891

[8] Yongzhi Cheng, Yan Nie, Zhengze Cheng, and Rong Zhou Gong. 2014. Dual-band Circular Polarizer and Linear Polarization Transformer Based on Twisted Split-Ring Structure Asymmetric Chiral Metamaterial. *Progress In Electromagnetics Research* 145 (2014), 263–272. https://doi.org/10.2528/PIER14020501

[9] Xingshuo Cui, Guangming Wang, Dengpan Wang, Xiaofeng Li, Tong Cai, and Kaiyue Liu. 2021. Ultra-broadband transmissive gradient metasurface based on the topologically coding optimization method. *Optics Express, Vol. 29, Issue 14, pp. 22136-22145* 29, 14 (jul 2021), 22136–22145. https://doi.org/10.1364/OE.426187

[10] Analog Devices. 2024. Analog Devices EVAL-TINYRAD. https://www.analog.com/en/resources/evaluation-hardware-and-software/evaluation-boards-kits/eval-tinyrad.html.

[11] Manideep Dunna, Kshitiz Bansal, Sanjeev Anthia Ganesh, Eamon Patamasing, and Dinesh Bharadia. 2023. R-fiducial: Millimeter Wave Radar Fiducials for Sensing Traffic Infrastructure. In *2023 IEEE 97th Vehicular Technology Conference (VTC2023-Spring)*. 1–7. https://doi.org/10.1109/VTC2023-Spring57618.2023.10199374

[12] Mahdi Fozi, Ahmad R Sharafat, and Mehdi Bennis. 2021. Fast MIMO beamforming via deep reinforcement learning for high mobility mmWave connectivity. *IEEE Journal on Selected Areas in Communications* 40, 1 (2021), 127–142.

[13] Kaustav A Gopinathan, Avanish Mishra, Baris R Mutlu, Jon F Edd, and Mehmet Toner. 2023. A microfluidic transistor for automatic control of liquids. *Nature* 622, 7984 (2023), 735–741.

[14] Nathaniel K. Grady, Jane E. Heyes, Dibakar Roy Chowdhury, Yong Zeng, Matthew T. Reiten, Abul K. Azad, Antoinette J. Taylor, Diego A. R. Dalvit, and Hou-Tong Chen. 2013. Terahertz Metamaterials for Linear Polarization Conversion and Anomalous Refraction. *Science* 340, 6138 (2013), 1304–1307. https://doi.org/10.1126/science.1235399 arXiv:https://www.science.org/doi/pdf/10.1126/science.1235399

[15] Hichem Guerboukha, Yasith Amarasinghe, Rabi Shrestha, Angela Pizzuto, and Daniel M. Mittleman. 2021. High-volume rapid prototyping technique for terahertz metallic metasurfaces. *Opt. Express* 29, 9 (Apr 2021), 13806–13814. https://doi.org/10.1364/OE.422991

[16] Yaomin He, Huafeng He, Changhua Hu, Junjun Yin, and Jian Yang. 2022. Polarization Analysis of Trihedral Corner Reflector With High-Frequency Approximation. *IEEE Transactions on Antennas and Propagation* 70, 10 (2022), 9607–9620. https://doi.org/10.1109/TAP.2022.3177536

[17] Jimmy G. D. Hester and Manos M. Tentzeris. 2016. Inkjet-Printed Flexible mm-Wave Van-Atta Reflectarrays: A Solution for Ultralong-Range Dense Multitag and Multisensing Chipless RFID Implementations for IoT Smart Skins. *IEEE Transactions on Microwave Theory and Techniques* 64, 12 (2016), 4763–4773. https://doi.org/10.1109/TMTT.2016.2623790

[18] Xiaojun Huang, Xiongwei Ma, Huanhuan Gao, Linyan Guo, and Xiaoyan Li. 2023. Ultra-wideband linear-polarization conversion metasurface with high-efficient asymmetric transmission. *Applied Physics A: Materials Science and Processing* 129, 4 (apr 2023), 1–9. https://doi.org/10.1007/s00339-023-06541-0

[19] Tatsuya Iizuka, Takuya Sasatani, Toru Nakamura, Naoko Kosaka, Masaki Hisada, and Yoshihiro Kawahara. 2023. MilliSign: mmWave-Based Passive Signs for Guiding UAVs in Poor Visibility Conditions. (oct 2023), 1–15. https://doi.org/10.1145/3570361.3613264

[20] Alejandro Jimenez-Saez, Martin Schusler, Mohammed El-Absi, Ali Alhaj Abbas, Klaus Solbach, Thomas Kaiser, and Rolf Jakoby. 2020. Frequency Selective Surface Coded Retroreflectors for Chipless Indoor Localization Tag Landmarks. *IEEE Antennas and Wireless Propagation Letters* 19, 5 (may 2020), 726–730. https://doi.org/10.1109/LAWP.2020.2975143

[21] Nicholas Junker, Jinqun Ge, Guoan Wang, and Sanjib Sur. 2022. Poster: FlexVAA: A Flexible, Passive Van Atta Retroreflector for Roadside Infrastructure Tagging and Identification. *SenSys 2022 - Proceedings of the 20th ACM Conference on Embedded Networked Sensor Systems* (nov 2022), 820–822. https://doi.org/10.1145/3560905.3568089

[22] Petr Kadera, Alejandro Jiménez-Sáez, Tom Burmeister, Jaroslav Lacik, Martin Schusbler, and Rolf Jakoby. 2020. Gradient-Index-Based Frequency-Coded Retroreflective Lenses for mm-Wave Indoor Localization. *IEEE Access* 8 (2020), 212765–212775. https://doi.org/10.1109/ACCESS.2020.3039986

[23] Petr Kadera, Alejandro Jimenez-Saez, Lisa Schmitt, Martin Schusler, Martin Hoffmann, Jaroslav Lacik, and Rolf Jakoby. 2021. Frequency Coded Retroreflective Landmark for 230 GHz Indoor Self-Localization Systems. *15th European Conference on Antennas and Propagation, EuCAP 2021* (mar 2021). https://doi.org/10.23919/EUCAP51087.2021.9410973

[24] Petr Kadera, Jesus Sanchez-Pastor, Alejandro Jimenez-Saez, Martin Schusler, Jaroslav Lacik, and Rolf Jakoby. 2021. QCTO Luneburg Lens-Based Retroreflective Tag Landmarks for mm-Wave Self-Localization Systems. *2021 IEEE-APS Topical Conference on Antennas and Propagation in Wireless Communications, APWC 2021* (aug 2021), 105–108. https://doi.org/10.1109/APWC52648.2021.9539571

[25] Subhajit Karmakar, Atsutse Kludze, and Yasaman Ghasempour. 2024. Meta-Sticker: Sub-Terahertz Metamaterial Stickers for Non-Invasive Mobile Food Sensing. In *Proceedings of the 21st ACM Conference on Embedded Networked Sensor Systems* (Istanbul, Turkiye) *(SenSys '23)*. Association for Computing Machinery, New York, NY, USA, 335–348.

https://doi.org/10.1145/3625687.3625815

[26] Atsutake Kosuge, Satoshi Suehiro, Mototsugu Hamada, and Tadahiro Kuroda. 2022. mmWave-YOLO: A mmWave imaging radar-based real-time multiclass object recognition system for ADAS applications. *IEEE Transactions on Instrumentation and Measurement* 71 (2022), 1–10.

[27] A. Lazaro, J. Lorenzo, R. Villarino, and D. Girbau. 2015. Modulated corner reflector using frequency selective surfaces for FMCW radar applications. *European Microwave Week 2015: "Freedom Through Microwaves", EuMW 2015 - Conference Proceedings; 2015 45th European Microwave Conference Proceedings, EuMC* (dec 2015), 111–114. https://doi.org/10.1109/EUMC.2015.7345712

[28] Wei Li, Yu Lan, Huanpeng Wang, and Yuehang Xu. 2021. Microwave polarizer based on complementary split ring resonators frequency-selective surface for conformal application. *IEEE Access* 9 (2021), 111383–111389. https://doi.org/10.1109/ACCESS.2021.3102942

[29] Zhaomei Liu, Bei Zhao, Chunhong Jiao, Lihua Zhao, and Xingxing Han. 2021. Broadband cross-polarization conversion metasurface based on cross-shaped resonators. *Applied Physics A: Materials Science and Processing* 127, 11 (nov 2021), 1–9. https://doi.org/10.1007/S00339-021-04994-9

[30] Fei Long, Shixing Yu, Na Kou, Can Zhang, Zhao Ding, and Zhengping Zhang. 2020. Wideband and high-efficiency planar chiral structure design for asymmetric transmission and linear polarization conversion. *Journal of Applied Physics* 127, 2 (jan 2020), 23104. https://doi.org/10.1063/1.5129912/566507

[31] Haofan Lu, Mohammad Hossein Mazaheri, Reza Rezvani, and Omid Abari. 2023. A Millimeter Wave Backscatter Network for Two-Way Communication and Localization. *SIGCOMM 2023 - Proceedings of the ACM SIGCOMM 2023 Conference* (sep 2023), 49–61. https://doi.org/10.1145/3603269.3604873

[32] Charles A. Lynch, Genaro Soto-Valle, Jimmy Hester, and Manos M. Tentzeris. 2023. MmIDs Enter the 3rd Dimension: A Camera Inspired Broadbeam High-Gain Retrodirective Backscatter Tag. *IEEE MTT-S International Microwave Symposium Digest* 2023-June (2023), 1069–1072. https://doi.org/10.1109/IMS37964.2023.10188156

[33] Ruichun Ma, Shicheng Zheng, Hao Pan, Lili Qiu, Xingyu Chen, Liangyu Liu, Yihong Liu, Wenjun Hu, and Ju Ren. 2024. AutoMS: Automated Service for mmWave Coverage Optimization using Low-cost Metasurfaces. In *Proceedings of the 30th Annual International Conference on Mobile Computing and Networking* (Washington D.C., DC, USA) *(ACM MobiCom '24)*. Association for Computing Machinery, New York, NY, USA, 62–76. https://doi.org/10.1145/3636534.3649347

[34] Mohammad Hossein Mazaheri, Alex Chen, and Omid Abari. 2021. mmTag: a millimeter wave backscatter network. In *Proceedings of the 2021 ACM SIGCOMM 2021 Conference* (Virtual Event, USA) *(SIGCOMM '21)*. Association for Computing Machinery, New York, NY, USA, 463–474. https://doi.org/10.1145/3452296.3472917

[35] Siddharth Mohan, Kshitiz Bansal, Manideep Dunna, and Dinesh Bharadia. 2023. Retroreflection with Amplification for Long Range mmWave Sensing. *mmNets 2023 - Proceedings of the 2023 The 7th ACM Workshop on Millimeter-Wave and Terahertz Networks and Sensing Systems, Part of: Mobicom 2023* 23 (oct 2023), 1–6. https://doi.org/10.1145/3615360.3625090

[36] Thi Minh Nguyen, Huu Lam Phan, Dinh Lam Vu, Thi Quynh Hoa Nguyen, and Jung Mu Kim. 2022. Ultra-wideband and high-efficiency cross-polarization conversion using a double split ring shaped metasurface for C, X, and Ku-band applications. *AIP Advances* 12, 11 (nov 2022), 115002. https://doi.org/10.1063/5.0125802/2819666

[37] John Nolan, Kun Qian, and Xinyu Zhang. 2021. RoS: passive smart surface for roadside-to-vehicle communication. In *Proceedings of the 2021 ACM SIGCOMM 2021 Conference* (Virtual Event, USA) *(SIGCOMM '21)*. Association for Computing Machinery, New York, NY, USA, 165–178. https://doi.org/10.1145/3452296.3472896

[38] Edwin Olson. 2011. AprilTag: A robust and flexible visual fiducial system. In *2011 IEEE International Conference on Robotics and Automation*. 3400–3407. https://doi.org/10.1109/ICRA.2011.5979561

[39] Hao Pan, Lili Qiu, Bei Ouyang, Shicheng Zheng, Yongzhao Zhang, Yi-Chao Chen, and Guangtao Xue. 2023. PMSat: Optimizing Passive Metasurface for Low Earth Orbit Satellite Communication. In *Proceedings of the 29th Annual International Conference on Mobile Computing and Networking*. 1–15.

[40] Wu Pan, Yongrui Li, Zhen Zhang, Bin Zhang, and Haizhu Li. 2023. Design and analysis of a multi-band and dual-functional terahertz wave polarization converter based on asymmetric cross-shaped metasurface. *Optics Communications* 530 (mar 2023), 129171. https://doi.org/10.1016/J.OPTCOM.2022.129171

[41] Akarsh Prabhakara, Tao Jin, Arnav Das, Gantavya Bhatt, Lilly Kumari, Elahe Soltanaghai, Jeff Bilmes, Swarun Kumar, and Anthony Rowe. 2023. RadarHD: Demonstrating Lidar-like Point Clouds from mmWave Radar. In *Proceedings of the 29th Annual International Conference on Mobile Computing and Networking*. 1–3.

[42] Kun Qian, Lulu Yao, Kai Zheng, Xinyu Zhang, and Tse Nga Ng. 2023. UniScatter: A Metamaterial Backscatter Tag for Wideband Joint Communication and Radar Sensing. *Proceedings of the Annual International Conference on Mobile Computing and Networking, MOBICOM* (jul 2023), 301–316. https://doi.org/10.1145/3570361.3592526

[43] Jesús Sanchez-Pastor, Alejandro Jiménez-Sáez, Martin Schuessler, and Rolf Jakoby. 2021. Frequency-coded spherical retroreflector for wide-angle indoor localization tag landmarks. *2021 4th International Workshop on Mobile Terahertz Systems, IWMTS 2021* (jul 2021). https://doi.org/10.1109/IWMTS51331.2021.9486810

[44] Jesus Sanchez-Pastor, Ahmed Kamel, Martin Schuler, Rolf Jakoby, and Alejandro Jimenez-Saez. 2024. Double-Notch Frequency-Coded Corner Reflectors for sub-THz Chipless RFID Tags. *IEEE Antennas and Wireless Propagation Letters* (2024). https://doi.org/10.1109/LAWP.2024.3404625

[45] Jesús Sánchez-Pastor, Martin Schüßler, Rolf Jakoby, and Alejandro Jiménez-Sáez. 2024. Double-Layer Frequency Selective Surface-based Corner Reflector for Indoor Self-localization Systems in the W-band. *18th European Conference on Antennas and Propagation, EuCAP 2024* (2024). https://doi.org/10.23919/EUCAP60739.2024.10501184

[46] Kamal Sarabandi and Tsen-Chieh Chiu. 1996. Optimum corner reflectors for calibration of imaging radars. *IEEE Transactions on antennas and Propagation* 44, 10 (1996), 1348–1361.

[47] Daniel J. Schroeder. 2000. Chapter 13 - Dispersing Elements and Systems. In *Astronomical Optics* (second edition ed.), Daniel J. Schroeder (Ed.). Academic Press, San Diego, 321–351. https://doi.org/10.1016/B978-012629810-9/50014-1

[48] Zhambyl Shaikhanov, Fahid Hassan, Hichem Guerboukha, Daniel Mittleman, and Edward Knightly. 2022. Metasurface-in-the-Middle Attack: From Theory to Experiment. In *Proceedings of the 15th ACM Conference on Security and Privacy in Wireless and Mobile Networks* (San Antonio, TX, USA) *(WiSec '22)*. Association for Computing Machinery, New York, NY, USA, 257–267. https://doi.org/10.1145/3507657.3528549

[49] Zijian Shao, Ruiyi Shen, William Xia, Yasaman Ghasempour, Kaushik Sengupta, and Sundeep Rangan. 2023. A Hybrid Antenna-Metasurface Architecture for mmWave and THz Massive MIMO. *Conference Record - Asilomar Conference on Signals, Systems and Computers* (2023), 1610–1616. https://doi.org/10.1109/IEEECONF59524.2023.10477069

[50] Elahe Soltanaghaei, Akarsh Prabhakara, Artur Balanuta, Matthew Anderson, Jan M. Rabaey, Swarun Kumar, and Anthony Rowe. 2021. Millimetro: mmWave retro-reflective tags for accurate, long range localization. In *Proceedings of the 27th Annual International Conference*

on Mobile Computing and Networking (New Orleans, Louisiana) *(MobiCom '21)*. Association for Computing Machinery, New York, NY, USA, 69–82. https://doi.org/10.1145/3447993.3448627

[51] Yiwen Song, Changhan Ge, Lili Qiu, and Yin Zhang. 2023. 2ACE: Spectral Profile-driven Multi-resolutional Compressive Sensing for mmWave Channel Estimation. In *Proceedings of the Twenty-fourth International Symposium on Theory, Algorithmic Foundations, and Protocol Design for Mobile Networks and Mobile Computing*. 41–50.

[52] Yiwen Song, Hao Pan, Longyuan Ge, Lili Qiu, Swarun Kumar, and Yi-Chao Chen. 2024. MicroSurf: Guiding Energy Distribution inside Microwave Oven with Metasurfaces. In *Proceedings of the 30th Annual International Conference on Mobile Computing and Networking*. 1346–1360.

[53] K. Trzebiatowski, M. Rzymowski, L. Kulas, and K. Nyka. 2020. 60 GHz microstrip van atta arrays for millimeter wave identification and localization. *2020 23rd International Microwave and Radar Conference, MIKON 2020* (oct 2020), 132–135. https://doi.org/10.23919/MIKON48703.2020.9253855

[54] Jingwen Wei, Yunping Qi, Baohe Zhang, Jinghui Ding, Weiming Liu, and Xiangxian Wang. 2022. Research on beam manipulate and RCS reduction based on terahertz ultra-wideband polarization conversion metasurface. *Optics Communications* 502 (jan 2022), 127425. https://doi.org/10.1016/J.OPTCOM.2021.127425

[55] Stephanie J Woodman, Dylan S Shah, Melanie Landesberg, Anjali Agrawala, and Rebecca Kramer-Bottiglio. 2024. Stretchable Arduinos embedded in soft robots. *Science Robotics* 9, 94 (2024), eadn6844.

[56] Lin-Sheng Wu, XiePeng Chen, JinLong Feng, and Jun-Fa Mao. 2023. Broadband electrically tunable linear polarization converter based on a graphene metasurface. *Optics Express, Vol. 31, Issue 2, pp. 1420-1431* 31, 2 (jan 2023), 1420–1431. https://doi.org/10.1364/OE.477907

[57] Kai-kai Xu, Zhong-yin Xiao, and Jing-yao Tang. 2017. Linearly polarized converters for reflected and transmitted waves based on double-split ring resonator. *Plasmonics* 12 (2017), 1869–1874. https://doi.org/10.1007/s11468-016-0456-2

[58] Wanchen Yang, Chenyu Zhou, Quan Xue, Qiye Wen, and Wenquan Che. 2021. Millimeter-wave frequency-reconfigurable metasurface antenna based on vanadium dioxide films. *IEEE Transactions on Antennas and Propagation* 69, 8 (2021), 4359–4369.

[59] Xiaoying Yang, Jacob Sayono, and Yang Zhang. 2023. CubeSense++: Smart Environment Sensing with Interaction-Powered Corner Reflector Mechanisms. In *Proceedings of the 36th Annual ACM Symposium on User Interface Software and Technology* (San Francisco, CA, USA) *(UIST '23)*. Association for Computing Machinery, New York, NY, USA, Article 78, 12 pages. https://doi.org/10.1145/3586183.3606744

[60] Xiaoying Yang and Yang Zhang. 2021. CubeSense: Wireless, Battery-Free Interactivity through Low-Cost Corner Reflector Mechanisms. In *Extended Abstracts of the 2021 CHI Conference on Human Factors in Computing Systems* (Yokohama, Japan) *(CHI EA '21)*. Association for Computing Machinery, New York, NY, USA, Article 386, 6 pages. https://doi.org/10.1145/3411763.3451599

[61] Zimeng Ye, Chao Tan, Xiaolei Huang, Yi Ouyang, Lei Yang, Zegao Wang, and Mingdong Dong. 2023. Emerging MoS2 wafer-scale technique for integrated circuits. *Nano-micro letters* 15, 1 (2023), 38.

[62] Hao Zhang, Binbin Wei, Jiduo Dong, Qing Zang, Chishen Huang, Xiangxing Bai, Linlong Tang, Haofei Shi, Chunheng Liu, Yang Liu, and Yueguang Lu. 2023. Tunable broadband transmissive terahertz cross-polarization converter enabled by a hybrid metal-graphene metasurface. *Results in Physics* 44 (jan 2023), 106190. https://doi.org/10.1016/J.RINP.2022.106190

[63] Xueqian Zhang, Zhen Tian, Weisheng Yue, Jianqiang Gu, Shuang Zhang, Jiaguang Han, and Weili Zhang. 2013. Broadband Terahertz Wave Deflection Based on C-shape Complex Metamaterials with Phase Discontinuities. *Advanced Materials* 25, 33 (sep 2013), 4567–4572. https://doi.org/10.1002/ADMA.201204850

[64] Rui Zhao, Haiyan Chen, Linbo Zhang, Fengxia Li, Peiheng Zhou, Jianliang Xie, and Longjiang Deng. 2018. Design and implementation of high efficiency and broadband transmission-type polarization converter based on diagonal split-ring resonator. *Progress in Electromagnetics Research* 161 (2018), 1–10. https://doi.org/10.2528/PIER17110604

[65] Yuting Zhao, Simone Genovesi, Guliano Manara, and Filippo Costa. 2022. Frequency-Coded mm-Wave RFID Tags Using Cross Polarization. In *2022 3rd URSI Atlantic and Asia Pacific Radio Science Meeting (AT-AP-RASC)*. 1–4. https://doi.org/10.23919/AT-AP-RASC54737.2022.9814422

[66] Kaichen Zhu, Chao Wen, Areej A Aljarb, Fei Xue, Xiangming Xu, Vincent Tung, Xixiang Zhang, Husam N Alshareef, and Mario Lanza. 2021. The development of integrated circuits based on two-dimensional materials. *Nature Electronics* 4, 11 (2021), 775–785.